École polytechnique fédérale de Lausanne (EPFL)

Faculté des sciences de base
Section de physique

Centre de Recherches en Physique des Plasmas (CRPP)

Association EURATOM
Confédération Suisse

Doctoral school

Stability of the internal kink mode for JET plasma scenarios described by an extended energy principle including kinetic additions

CRPP internal report
INT 210/04

Christian SCHLATTER

PPB 310
CH-1015 Lausanne
Switzerland

2004, 24^{th} of October

Made with LaTeX 2_ε

Contents

List of Figures

Chapter 1

Instability of the internal kink mode

1.1 The internal kink mode

Magnetohydrodynamics (MHD) predicts instabilities in tokamak plasmas. In a perfectly conducting plasma, described by ideal MHD, the presence of current and pressure gradients can lead to, among others, kink modes, which cause a displacement of the magnetic surfaces of constant flux. More specific, the internal kink mode has the topology of an $m = 1$, $n = 1$ mode, therefore, as $m = nq$, its resonant surface is located at the $q = 1$ surface, displacing the plasma contained inside the volume delimited by that surface.

These modes are experimentally observed on various plasma reactors, their presence results in sawteething plasma parameters. Sawteeth lead to energy loss of the plasma and therefore lower its confinement. With increasing pressure, the instabilities exceed the limit to let the plasma recover. As it will be shown in the following, theory predicts a pressure threshold for the stability of the plasma [4].

1.2 Conditions for stability of the mode

The stability of the internal kink mode is evident if $\min(q(r)) > 0$ since there will be no layer in the plasma where the mode could build up.

In the presence of a resonant surface the stability of the mode can be analyzed using the 'energy principle', a concept based on a variational formulation of the equations of motion of the plasma [2]. The principle reflects the fact that if a physically allowable perturbation of an equilibrium lowers the potential energy, then the equilibrium is unstable.

The energy change caused by a displacement $\xi(x)$ due to a force $\mathbf{F}(x)$ of the plasma is defined by the volume integral

$$\delta W = -\frac{1}{2}\int \xi \cdot \mathbf{F}\, d^3x \tag{1.1}$$

By expressing the perturbed quantities of the plasma in terms of the displacement for a volume inside the plasma, δW is written as [11]

$$\delta W = \frac{1}{2}\int_{plasma} \left(\gamma\, p_0 \left(\nabla \cdot \xi\right)^2 + \left(\xi \cdot \nabla p_0\right) \nabla \cdot \xi + \frac{B_1^2}{\mu_0} - \mathbf{j_0} \cdot \left(\mathbf{B_1} \times \xi\right) \right) d^3x \tag{1.2}$$

where the subscript 0 and 1 refer to the equilibrium and the perturbation respectively.

To study the stability of the internal kink it is convenient to develop equation 1.2 and the displacement in orders of ε, the aspect ratio of the tokamak $\varepsilon = a/R \ll 1$

$$\delta W = \delta W_0 + \delta W_2 + \delta W_4 \tag{1.3}$$

$$\xi = \xi_0 + \xi_1 + \xi_2 \tag{1.4}$$

permitting to approximate further for a low pressure scenario with $q \propto \mathcal{O}(1)$, $p \propto \delta W(\varepsilon^2)$ and $B_\phi \propto \delta W(1)$.

In the toric tokamak, a perturbation of the flux surfaces is constraint by its poloidal and toroidal periodicity and may therefore be written as a Fourier series

$$\xi(r,\theta,\phi) = \sum_m \xi(r,m) \exp\left(i\left(m\theta - n\phi - \omega t\right)\right) \tag{1.5}$$

In zeroth order of ε [7], assuming perpendicular incompressibility, the integral

$$\delta W_0 = \frac{1}{2}\int d^3x \frac{B^2}{\mu_0}\left(\nabla \cdot \xi_\perp\right)^2 \tag{1.6}$$

vanishes. Instability must come from higher orders. In the frame of the low β approximation, δW_2 writes

$$\delta W_2 = \frac{2\pi^2 B_0^2}{\mu_0 R_0}\int_0^a dr\; r^3 \left(\frac{d\xi_{r0}}{dr}\right)^2 \left(1 - \frac{1}{q}\right)^2 \tag{1.7}$$

for the $m = 1$ mode.

For constant displacement $\frac{d\xi_{r0}}{dr} = 0$ (except for the singular layer at r_1, see figure 1.1) the integral is positive definite and reduces to zero for $q(r_1) = 1$. Therefore, the internal kink is marginally stable to ε^2.

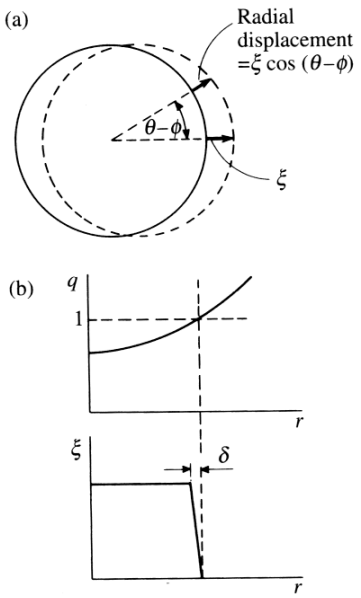

Figure 1.1: Displacement ξ

(a) shows the displacement of a circular flux surface for an m = 1 perturbation. **(b)** shows the radial dependence of ξ for an unstable displacement.

Rosenbluth et al. [10] showed that, for a cylindrical geometry, δW_4 is minimized to zero too.

Bussac [4] demonstrated that the inclusion of toroidal effects (like the Shafranov-shifted flux surfaces) leads to the loss of stability for the ideal internal $m = n = 1$ kink mode. For quadratic safety factor profiles a poloidal $\beta_p \geqslant \beta_p^c \approx 0.3$ makes the internal kink mode unstable.

A more realistic calculation (with a plasma surrounded by a vacuum layer) shows a stronger trend towards instability, [3] gives a critical β-threshold profile which cancels for an inversion radius $r_1 \approx 0.5$ .. $0.9\ a$.

Chapter 2

Stabilisation of the mode

Experiments in JET showed that the presence of energetic, trapped or passing particles can stabilize the internal kink mode [5], [6], [9] and [12]. Figure 2.1 shows a JET plasma, whose sawtooth activity is stabilized by the application of ICRF and NBI heating. The kinetics of the created fast particle populations permit to have a sawteeth-free tokamak even at high β.

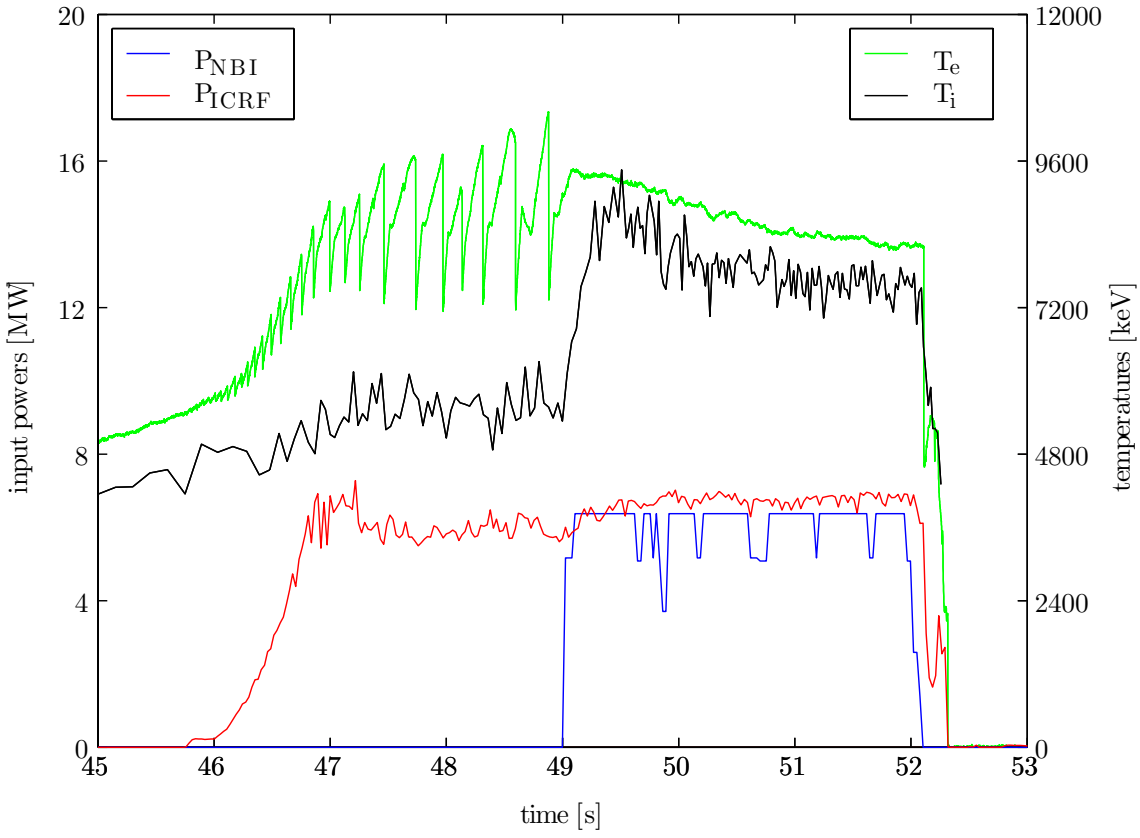

Figure 2.1: Behaviour of central electron and ion temperatures during the longest period of sawteeth stabilization observed in JET. When the neutral beam power (blue curve) is applied to the plasma, the sawteeth on the electron temperature (green curve) disappear and the confinement improves by about 20 % during a stationary phase of more than 3 seconds. The data shown was acquired with JET plasma discharge #15697 with $I_p = 3$ MA, $B_\phi = 3.15$ T.

To account for the effect of these particles, a kinetic contribution is added to the energy principle of the ideal MHD. J. Graves devoted his thesis [7] to this subject.

2.1 Extension of the energy principle

The ideal MHD energy principle (equation 1.2, noted fluid term δW_f) is completed by a kinetic contribution, δW_k,

$$\delta W = \delta W_f + \delta W_k \tag{2.1}$$

with

$$\delta W_k = \frac{1}{2}\int d^3x\ \xi^* \cdot (\nabla \cdot \delta \mathbb{P}_k) \tag{2.2}$$

where $\mathbb{P}_k$ is the kinetic contribution of the energetic thermal ions to the perturbed ion pressure tensor (chapter 3.3 in [7]). The extension of the energy principle is valid for the description of the ideal internal kink stability boundary for the regime of collisionless ion populations. As the critical boundary for stability lies in the outer regions of the plasma, the analysis must only include that region. This results in (equation 3.59 in [7])

$$\delta W_k = -2^{7/2}\pi^3 m_i \left(\frac{\xi_0}{R_0}\right)^2 \int_0^{r_1} dr\ r^2 \int_0^1 dk^2 \frac{I_q^2}{K_b} \int_0^\infty d\varepsilon\ \varepsilon^{5/2}\frac{\partial f_i}{\partial \varepsilon}\left[\frac{\omega - \omega_{*i}}{\omega - \langle\omega_{mdi}\rangle}\right] \tag{2.3}$$

where ω_{*i} is the non-local ion diamagnetic frequency and k^2 is the pitch angle variable defined by

$$k^2 = \frac{1 + \alpha B_0\,(\epsilon - 1)}{2\epsilon\alpha B_0}, \quad \alpha = \frac{\mu}{\varepsilon} \tag{2.4}$$

and $\langle\omega_{mdi}\rangle$ the bounce averaged magnetic precession drift frequency

$$\langle\omega_{mdi}\rangle = \frac{m_i q(r)\varepsilon}{eZ_{eff} r B_0 R_0}\left[F_1\left(k^2\right) + 2s(r)F_2\left(k^2\right) - \zeta\left(\frac{1}{4q^2} + F_3\left(k^2\right)\right)\right] \tag{2.5}$$

with $q(r)$ the safety factor profile, Z_{eff} the effective plasma charge,

$$s(r) = \frac{r}{q}\frac{dq}{dr} \tag{2.6}$$

the magnetic shear and the functions

$$F_1 = \frac{2E\left(k^2\right)}{K\left(k^2\right)} - 1 \tag{2.7}$$

$$F_2 = \frac{2E\left(k^2\right)}{K\left(k^2\right)} + 2\left(k^2 - 1\right) \tag{2.8}$$

$$F_3 = \frac{4}{3}\left(\left(\left(2k^2 - 1\right)\right)\frac{E\left(k^2\right)}{K\left(k^2\right)} + \left(1 - k^2\right)\right) \tag{2.9}$$

where ζ reflects the modification of $\langle\omega_{mdi}\rangle$ due to the shifting of the magnetic surfaces, characterized by

$$\zeta = -\frac{2R\mu_0}{B^2}\frac{dp}{dr}q^2 \tag{2.10}$$

where $K\left(k^2\right)$ and $E\left(k^2\right)$ are the complete elliptic integrals of the first and second kind respectively [1]. Further,

$$K_b\left(k^2\right) = \frac{1}{\pi}\sqrt{\frac{2}{\varepsilon}}K\left(k^2\right) \tag{2.11}$$

and[1]

$$I_q\left(r,k^2\right)=\frac{1}{\pi}\sqrt{\frac{2}{\varepsilon}}F_q\left(q,k^2\right) \tag{2.12}$$

with

$$\begin{aligned}F_q\left(q,k^2\right)=2E\left(k^2\right)-K\left(k^2\right)-\frac{4(1-q)cos(\pi q)}{1-4(1-q)^2}\left(E\left(k^2\right)+\left(k^2-1\right)K\left(k^2\right)\right)\\ -(1+cos(\pi q))f_1(q)\left(E\left(k^2\right)+\left(k^2-1\right)K\left(k^2\right)+\frac{2}{\pi}E\left(k^2\right)-1\right)\\ -(1+cos(\pi q))\left(E\left(k^2\right)-K\left(k^2\right)\right)-f_2(q)(1-\left(k^2\right))\left(\frac{\pi}{2}-K\left(k^2\right)\right)\end{aligned} \tag{2.13}$$

where

$$f_1(q)=\frac{\pi}{2}\left(1.0841-0.3193(1-q)^2-0.0683(1-q)^4\right) \tag{2.14}$$

and

$$f_2(q)=5.1\left(q-\frac{1}{2}\right)(1-q)^2\left(1-0.034(1-q)\right) \tag{2.15}$$

J. Graves developed an analytic reduction of equation 2.3 which is reproduced in appendix A and subsequently used for the calculations presented in the next chapter.

[1] this is equation 6.21 which interpolates equation 3.60, [7]

Chapter 3

Calculation of δW_k for JET parameters

3.1 Input parameters

The real and imaginary parts of δW_k have been calculated for parameters which are characteristic for JET. The following generic expressions for q-profile, toroidal magnetic field, pressure gradient, plasma rotation, ion temperature and density have been used:

$$q(r) = q_0 \left(1 + d\left(\frac{r}{a}\right)^{2c}\right)^{1/c} \tag{3.1}$$

$$B_\phi(r) = B_0 \left(\frac{R_0}{R_0 + r}\right) \tag{3.2}$$

$$\frac{dp}{dr} = -\frac{B_\phi(r)}{\mu_0}\frac{dB}{dr} \tag{3.3}$$

$$\Omega_r = \Omega_0 \left(1 - \left(\frac{2r}{a}\right)^2\right) \tag{3.4}$$

$$T_i(r) = T_{i0}\left(1 - \left(\frac{r}{a}\right)^2\right) + T_{ia} \tag{3.5}$$

$$n_i(r) = n_{i0}\left(1 - \left(\frac{r}{a}\right)^2\right)^{\nu_n} \tag{3.6}$$

The derivatives of the above quantities were calculated analytically for the points of the grid (if necessary).

3.2 Results and conclusions

δW_k was calculated for a set of parameters $B_0 = 3$ T, $R_0 = 2.96$ m, a = 1.25 m, $Z_{eff} = 1$, $q_0 = 0.7$, $c = 1.33$, $d = 9.09$, $T_{i0} = 2$ keV, $T_{ia} = 50$ eV, $n_{i0} = 4{\cdot}10^{-19}$ m^{-3}, $\nu_n = 6$; resulting in $r_1 = 0.45$ m. Figure 3.1 shows a compilation of these radial profiles for $r \in [0, r_1]$.

The calculation was carried out on a grid of 1000×1000 points, equally spaced and spanning the intervals $r = [0;\, r_1]$ and $k^2 = [0;\, 1]$ respectively.

The plots do not include rotation of the plasma, i.e. $\Omega_0 = 0$.

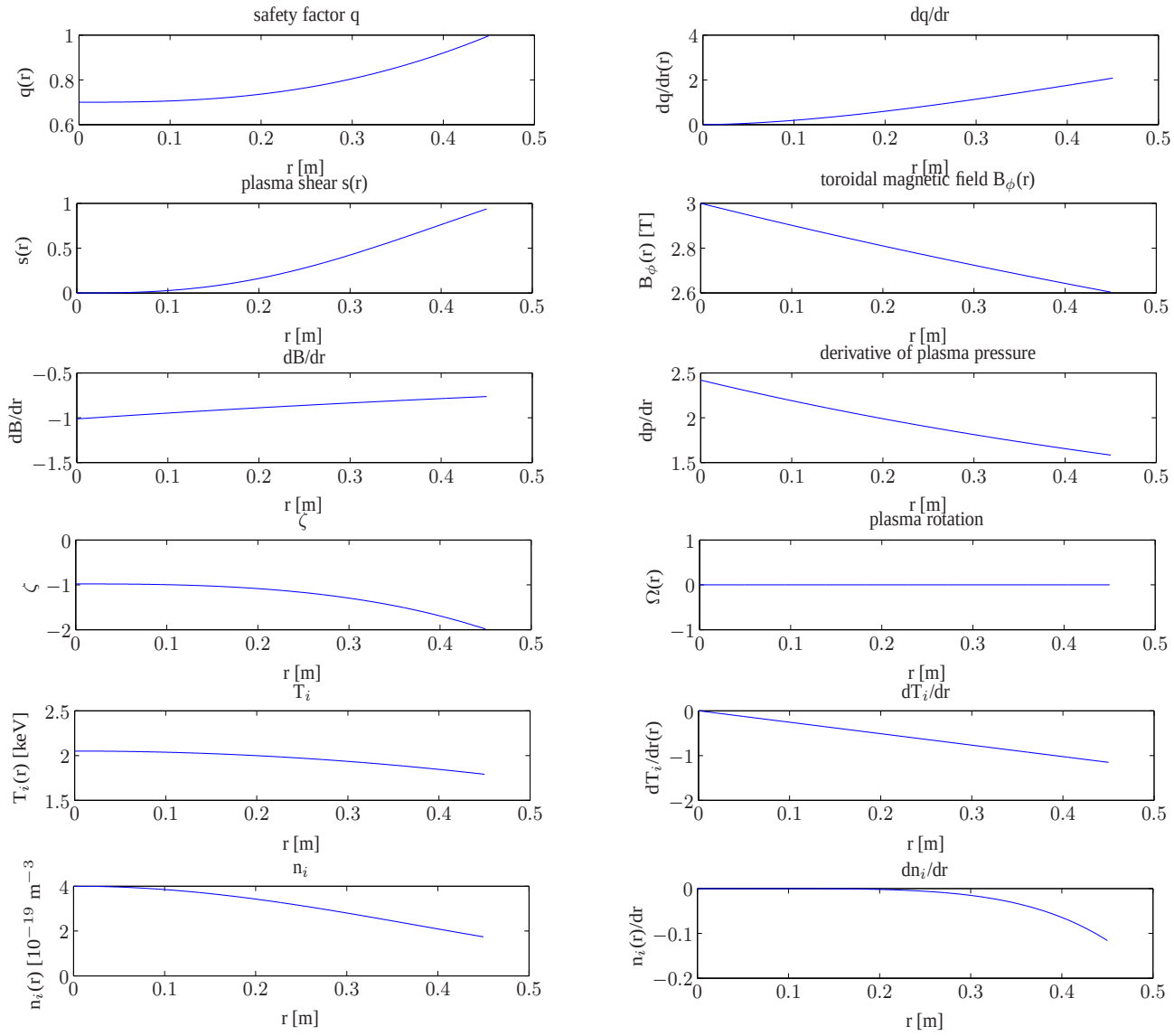

Figure 3.1: Parametric input parameter profiles for the simulation. From top left to right bottom are plotted: $q(r)$, $\frac{dq}{dr}$, $s(r)$, $B_\phi(r)$, $\frac{dB}{dr}$, $\frac{dp}{dr}$, $\eta(r)$, $\Omega(r)$, $T_i(r)$, $\frac{dT_i}{dr}$, $n_i(r)$ and $\frac{dn_i}{dr}$.

Figure 3.2 shows the real and imaginary part of δW_k for the selected parameters. Indeed the kinetic contribution to δW is positive, stabilizing the mode for a large range of possible mode frequencies. Whilst the real part of δW identifies the pure mode growth rate γ, its imaginary part characterizes the mode rotation frequency (as a consequence of the Landau resonance of barely precessing ions) $\omega_r = \Im(\omega)$ at marginal stability.

In [7] the solution of the dispersion relation gives two types of existing modes, one of which is located in the Alfvén continuum ($\tilde{\omega} > \tilde{\omega_{*pi}}$ or $\tilde{\omega} < 0$) and whose imaginary dispersion relation writes

$$\Im\left\{D\left(\tilde{\omega}\right)\right\} = \left.\frac{s\sqrt{1+\Delta}}{3\pi\varepsilon^2}\frac{\sqrt{\tilde{\omega}\left(\tilde{\omega}-\omega_{*pi}\right)}}{\omega_A}\right|_{r_1} - \Im\left\{\delta\hat{W}_k\right\} = 0 \tag{3.7}$$

and the other mode, called *gap mode* with $0 < \tilde{\omega} < \tilde{\omega_{*pi}}$ giving

$$\Im\left\{D\left(\tilde{\omega}\right)\right\} = 0 \tag{3.8}$$

As $\Im\{D(\tilde{\omega})\} > 0$ in figure 3.2 the gap mode will not propagate. The frequency of the Alfvén mode could be determined using equation 3.7.

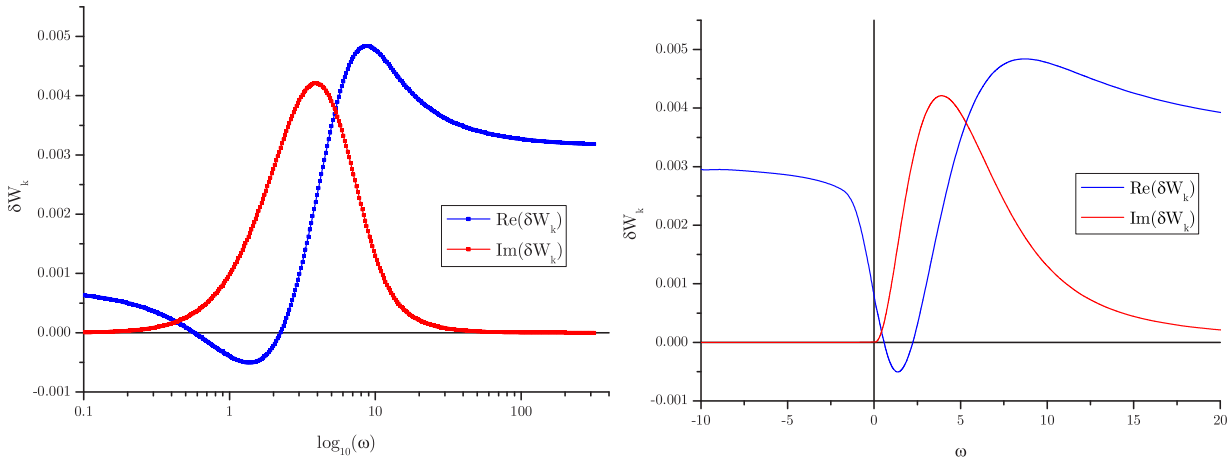

Figure 3.2: $\delta\mathbf{W}_k$ as a function of the mode frequency. Plotted are the real (blue curve) and imaginary part (red curve) for the input parameters stated in the text. The left figure shows a plot versus logarithmic scale of the mode frequency, the right figure shows the same result with linear scale of ω.

If we add a strong pressure (gradient) at q=1 by setting $\eta = 2$, the imaginary part of $\delta\mathrm{W}_k$ gets strongly negative for small negative mode frequencies, meaning that the resonance is caused by inverse precessing ions. This is plotted in figure 3.3. At $\omega = 0$ the kinetic effects destabilize the mode.

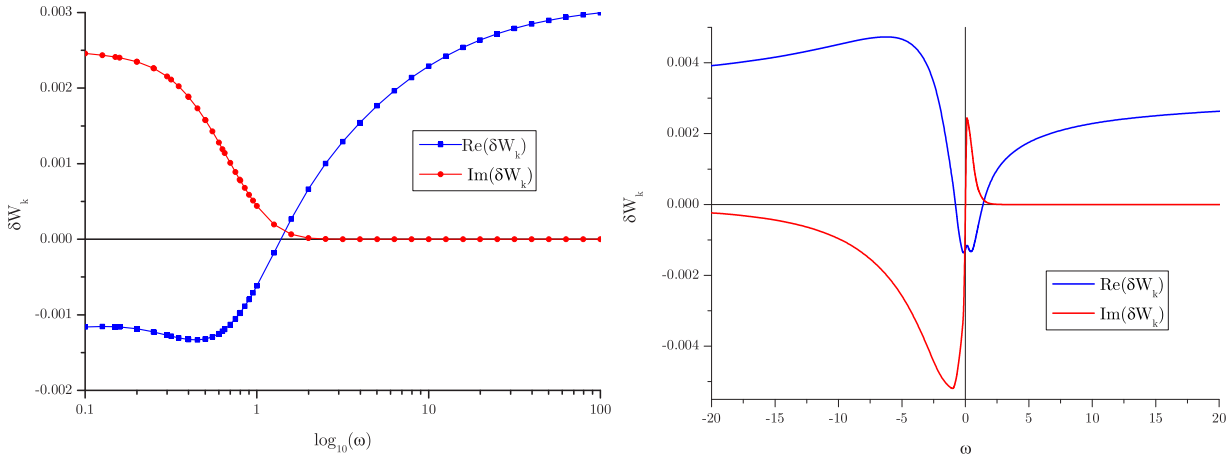

Figure 3.3: $\delta\mathbf{W}_k$ as a function of the mode frequency for $\eta = 2$. Plotted are the real (blue curve) and imaginary part (red curve) as in figure 3.2.

3.3 Future work

For the future, the code should be extended to include anisotropic distribution functions (see equation A.2) with an exponent argument $b(r, k)$ depending on radius and pitch angle compatible with fast ion populations in plasmas heated by ICRF.

Further, the code could entirely be implemented in Fortran, to lower execution time.

An interface to fetch JET PPF data could replace the analytic profile expressions used so far.

Once done all this, scans in all relevant plasma parameters could then easily carried out and the code could be integrated in existing MHD codes to account for the kinetic effects affecting stability.

Appendix A

Analytic reduction of δW_k

This is a reproduction of the appendix B of [7]. This appendix describes the analytical methods used to reduce the complexity of $\Re\{\delta\hat{W}_{ki}\}$ and $\Im\{\delta\hat{W}_{ki}\}$.
The kinetic perturbed potential energy term of equation 2.3, accounting for the rotation of the plasma $\Omega_\phi(r)$ can be written in the form,

$$\delta W_{ki} = -2^{\frac{7}{2}}\pi^3|\xi_{r0}|^2 m_i \frac{1}{R_0^2}\int_0^{r_1} dr r^2 \int_0^\infty d\mathcal{E}\mathcal{E}^{\frac{5}{2}} \int_0^1 dk^2 \frac{I_q^2\left(\omega_{tot}\frac{\partial f_i}{\partial \mathcal{E}} - \frac{q}{r\omega_{ci}}\frac{\partial f_i}{\partial r}\right)}{K_b[\omega_{tot} - \overline{\omega}_{mdi}]}, \tag{A.1}$$

with $\omega_{tot}(r) = \omega - \Omega_\Phi(r) = \tilde{\omega} + \Omega_\Phi(r_1) - \Omega_\Phi(r)$ and $\omega_{ci} = eZB_0/m_i$. The energy integral can be evaluated analytically if the ions are distributed negative exponentially. Such distributions describe ICRH and thermal ion populations:

$$f_i(r,k,\mathcal{E}) = N(r,k)\exp(-b(r,k)\mathcal{E}), \tag{A.2}$$

where $b = m_i/T_i$ and $N = n_i m_i^{3/2}/(2\pi T_i)^{3/2}$ for a Maxwellian thermal ion population. By substituting Eq. (A.2) into Eq. (A.1), δW_{ki} contains energy integrals of the form,

$$\int_0^\infty \frac{\mathcal{E}^{\frac{5}{2}}\exp(-b\mathcal{E})}{\omega_{tot} - \mathcal{D}\mathcal{E}} d\mathcal{E}\ ,\ \int_0^\infty \frac{\mathcal{E}^{\frac{7}{2}}\exp(-b\mathcal{E})}{\omega_{tot} - \mathcal{D}\mathcal{E}} d\mathcal{E} \tag{A.3}$$

where $\langle\omega_{mdi}\rangle = \mathcal{D}(r,k)\mathcal{E}$. At marginal stability

$$\begin{aligned}
\Re\left\{\int_0^\infty \frac{\mathcal{E}^{\frac{5}{2}}\exp(-b\mathcal{E})}{\omega_{tot} - \mathcal{D}\mathcal{E}} d\mathcal{E}\right\} &= \frac{\sqrt{\pi}}{4b^{\frac{7}{2}}\omega_{tot}}\mathrm{Fn}_1(x), \\
\Re\left\{\int_0^\infty \frac{\mathcal{E}^{\frac{7}{2}}\exp(-b\mathcal{E})}{\omega_{tot} - \mathcal{D}\mathcal{E}} d\mathcal{E}\right\} &= \frac{\sqrt{\pi}}{4b^{\frac{9}{2}}\omega_{tot}}\mathrm{Fn}_2(x), \\
\Im\left\{\int_0^\infty \frac{\mathcal{E}^{\frac{5}{2}}\exp(-b\mathcal{E})}{\omega_{tot} - \mathcal{D}\mathcal{E}} d\mathcal{E}\right\} &= -\frac{\pi}{\omega_{tot}b^{\frac{7}{2}}}\mathrm{Fn}_3(x), \\
\Im\left\{\int_0^\infty \frac{\mathcal{E}^{\frac{7}{2}}\exp(-b\mathcal{E})}{\omega_{tot} - \mathcal{D}\mathcal{E}} d\mathcal{E}\right\} &= -\frac{\pi}{\omega_{tot}b^{\frac{9}{2}}}\mathrm{Fn}_4(x),
\end{aligned} \tag{A.4}$$

with $x = \mathcal{D}/(b\,\omega_{tot})$. For $x > 0$, trapped ions magnetically precess in the same direction as ω_{tot} giving

$$\begin{aligned}
\mathrm{Fn}_{1+}(x) &= 4\sqrt{\pi}\frac{1}{x^{\frac{7}{2}}}\mathrm{erfi}\left(\frac{1}{\sqrt{x}}\right)\exp\left(-\frac{1}{x}\right) - \frac{3}{x} - \frac{2}{x^2} - \frac{4}{x^3},\\
\mathrm{Fn}_{2+}(x) &= 4\sqrt{\pi}\frac{1}{x^{\frac{9}{2}}}\mathrm{erfi}\left(\frac{1}{\sqrt{x}}\right)\exp\left(-\frac{1}{x}\right) - \frac{15}{2x} - \frac{3}{x^2} - \frac{2}{x^3} - \frac{4}{x^4},\\
\mathrm{Fn}_{3+}(x) &= \frac{1}{x^{7/2}}\exp\left[-\frac{1}{x}\right],\\
\mathrm{Fn}_{4+}(x) &= \frac{1}{x^{9/2}}\exp\left[-\frac{1}{x}\right],
\end{aligned} \tag{A.5}$$

where '+' denotes $x > 0$,

$$\mathrm{erfi}(x) = -i\mathrm{erf}(ix) = \frac{2}{\sqrt{\pi}}\int_0^x \exp(z^2)dz,$$

and $\mathrm{erf}(x)$ is the standard error function [1].
For $x < 0$, the energy integral does not contain a residue. This follows from the fact that the resonance condition $\omega_{tot} = \mathcal{D}\mathcal{E}$ cannot be met for any energy or radius if $x \propto \mathcal{D}/\omega_{tot} < 0$. However, the principle parts of Eq. (A.3) do not vanish:

$$\begin{aligned}
\mathrm{Fn}_{1-} &= -4\sqrt{\pi}\frac{1}{(-x)^{\frac{7}{2}}}\mathrm{erfc}\left(\frac{1}{\sqrt{-x}}\right)\exp\left(-\frac{1}{x}\right) - \frac{3}{x} - \frac{2}{x^2} - \frac{4}{x^3},\\
\mathrm{Fn}_{2-} &= +4\sqrt{\pi}\frac{1}{(-x)^{\frac{9}{2}}}\mathrm{erfc}\left(\frac{1}{\sqrt{-x}}\right)\exp\left(-\frac{1}{x}\right) - \frac{15}{2x} - \frac{3}{x^2} - \frac{2}{x^3} - \frac{4}{x^4},\\
\mathrm{Fn}_{3-} &= 0,\\
\mathrm{Fn}_{4-} &= 0,
\end{aligned} \tag{A.6}$$

where '−' denotes $x < 0$ and $\mathrm{erfc}(x) = 1 - \mathrm{erf}(x)$. From inspection of Eqs. (A.5) and (A.6), numerical difficulties are clearly envisaged at the pitch angle k_c^2 for which the magnetic precession drift of trapped ions is nullified; i.e. k_c^2 is defined by $x(k_c) = 0$. However, one can show that in the limit $x \to 0$ (or $k^2 \to k_c^2$), Fn_3 and Fn_4 vanish and Fn_1 and Fn_2 converge. Specifically, $\mathrm{Fn}_{1+}(k^2 = k_c^2) = \mathrm{Fn}_{1-}(k^2 = k_c^2) = 15/2$ and $\mathrm{Fn}_{2+}(k^2 = k_c^2) = \mathrm{Fn}_{2-}(k^2 = k_c^2) = 105/4$. To remove the numerical difficulties that arise from the cancellation of singular terms as $x \to 0$, Fn_1 and Fn_2 are numerically interpolated within the range $-1 < x < 1$.

The following normalised quantities are now used:

$$\hat{n}_i = n_i/10^{19}\,\mathrm{m}^{-3}$$

$$\hat{T}_i = T_i/1\mathrm{keV}$$

$$\hat{\omega}_{tot} = \omega_{tot}/1\mathrm{k}\ \mathrm{rs}^{-1}.$$

Hence, referring to Eq. 2.5 for the definition of $\langle\omega_{mdi}\rangle$, yields

$$x(r,k^2) = \frac{q(r)\hat{T}_i(r)\left[F_1(k^2) + 2s(r)F_2(k^2) - \zeta(r)\left(\frac{1}{4q(r)^2} + F_3(k^2)\right)\right]}{B_0R_0Zr\hat{\omega}_{tot}(r)}, \tag{A.7}$$

and recalling the normalisation $\delta W = 6\pi^2 R_0 B_0^2 \xi_0^2 \varepsilon_1^4 \delta\hat{W}/\mu_0$, one can now show that

$$\Re\left\{\delta\hat{W}_{ki}\right\} = 0.151\times10^{-3}\left(\frac{1}{B_0^2\varepsilon_1^{3/2}r_1^{5/2}}\right)\int_0^{r_1} dr r^{\frac{1}{2}} \times\left[\left\{\frac{q\hat{T}_i}{B_0 Z\hat{\omega}_{tot}}\left(\hat{T}_i\frac{d\hat{n}_i}{dr}-\frac{3}{2}\hat{n}_i\frac{d\hat{T}_i}{dr}\right)+\hat{n}_i\hat{T}_i r\right\}\mathrm{G}_1+\frac{q\hat{n}_i\hat{T}_i}{B_0 Z\hat{\omega}_{tot}}\frac{d\hat{T}_i}{dr}\mathrm{G}_2\right] \tag{A.8}$$

where $0.151\times10^{-3} = \frac{e\mu_0\times10^{22}}{3\sqrt{2}\,\pi}$, and

$$\mathrm{G}_1(r) = \int_0^1 \frac{F_q^2}{K(k^2)}\mathrm{Fn}_1\, dk^2 \;\text{ and }\; \mathrm{G}_2(r) = \int_0^1 \frac{F_q^2}{K(k^2)}\mathrm{Fn}_2\, dk^2, \tag{A.9}$$

with F_q defined by Eq. 2.13.
The pitch angle integrals are arranged as follows,

$$\mathrm{G}_1(r) = \int_{k_a}^{k_b}\frac{F_q^2}{K(k^2)}\mathrm{Fn}_{1+}\, dk^2 + \int_{k_d}^{k_e}\frac{F_q^2}{K(k^2)}\mathrm{Fn}_1\, dk^2 + \int_{k_f}^{k_g}\frac{F_q^2}{K(k^2)}\mathrm{Fn}_{1-}\, dk^2, \tag{A.10}$$

where Fn_1 is interpolated between the limits k_d and k_e which correspond to the interval $-1 < x < 1$. Numerical values are assigned to the integral limits of Eq. (A.10) by noting that $\langle\omega_{mdi}\rangle$ (and therefore $|x|$) is in general a monotonically decreasing function of k^2 (at least for moderate values of ζ). For $\omega_{tot}(r) > 0$, the integration limits are defined: $k_a = 0$, $x(k_b) = x(k_d) = 1$, $x(k_e) = x(k_f) = -1$, $k_g = 1$. For $\omega_{tot}(r) < 0$, the integration limits are defined: $k_f = 0$, $x(k_e) = x(k_a) = 1$, $x(k_g) = x(k_d) = -1$, $k_b = 1$.
Since x is a function of r and k^2, then the limits k_a, k_b, k_d, k_e, k_f and k_g are also functions of r. Depending on the type of mode and the direction of the toroidal rotation, the sign of $\omega_{tot}(r)$ may change with respect to r and hence the definitions of the pitch angle integral limits must change appropriately throughout the radial integration.
The normalised imaginary kinetic potential energy is

$$\Im\left\{\delta\hat{W}_{ki}\right\} = -1.071\times10^{-3}\left(\frac{1}{B_0^2\varepsilon_1^{3/2}r_1^{5/2}}\right)\int_0^{r_1} dr r^{\frac{1}{2}} \times\left[\left\{\frac{q\hat{T}_i}{B_0 Z\hat{\omega}_{tot}}\left(\hat{T}_i\frac{d\hat{n}_i}{dr}-\frac{3}{2}\hat{n}_i\frac{d\hat{T}_i}{dr}\right)+\hat{n}_i\hat{T}_i r\right\}\mathrm{G}_3+\frac{q\hat{n}_i\hat{T}_i}{B_0 Z\hat{\omega}_{tot}}\frac{d\hat{T}_i}{dr}\mathrm{G}_4\right] \tag{A.11}$$

where $-1.071\times10^{-3} = \frac{2\sqrt{2}e\mu_0\times10^{22}}{3\sqrt{\pi}}$, and G_3 and G_4 are defined as follows. For $\omega_{tot}(r) > 0$:

$$\mathrm{G}_3(r) = \int_0^{k_c}\frac{F_q^2}{K(k^2)}\mathrm{Fn}_3\, dk^2 \;\text{ and }\; \mathrm{G}_4(r) = \int_0^{k_c}\frac{F_q^2}{K(k^2)}\mathrm{Fn}_4\, dk^2, \tag{A.12}$$

and for $\omega_{tot}(r) < 0$:

$$\mathrm{G}_3(r) = \int_{k_c}^1\frac{F_q^2}{K(k^2)}\mathrm{Fn}_3\, dk^2 \;\text{ and }\; \mathrm{G}_4(r) = \int_{k_c}^1\frac{F_q^2}{K(k^2)}\mathrm{Fn}_4\, dk^2. \tag{A.13}$$

The latter definitions of G_3 and G_4 emerge from the resonance of reverse magnetically precessing particles and thus tend to be small.

Appendix B

Implementation

Radial profiles are stored as row vectors of length n, pitch angle dependent quantities as column vectors of length m. Expressions depending on both r and k^2 are stored in a matrix m×n.

The integration of the integral A.1 is done by summing along the column (pitch angle integration) then by summing up the rows (integration over the radius).

The procedure is repeated for different values of the mode frequency.
Special care is taken of the evaluation of the functions F_{n1} and F_{n2} close to the singularity at $x = 0$. Figure B.1 shows the behavior the functions in the interpolated region around the origin.

B.1 Sourcecode

Listing B.1: Main program code

```
% simulation of marginally stable internal kink modes
%
clear all;
warning('off','MATLAB:divideByZero')
% parameters
% unperturbed toroidal magnetic field
B_0= 3; %toroidal magnetic field, [T], max 3.5
R_0= 2.96; %major radius, [m]
a=1.25; %minor limiter radius, [m]
r_1= 0.45; % can be calculated from q profile
%minor inversion radius (location of q=1 surface)
Z_eff=1;
epsilon_1=r_1/R_0;
e=1.6022E-19; %electron charge
mu_0=4*pi*1E-7;

% calculation grid definition
numradialpoints=1000;
numpitchanglepoints=1000;

rspacing=r_1./numradialpoints;
```

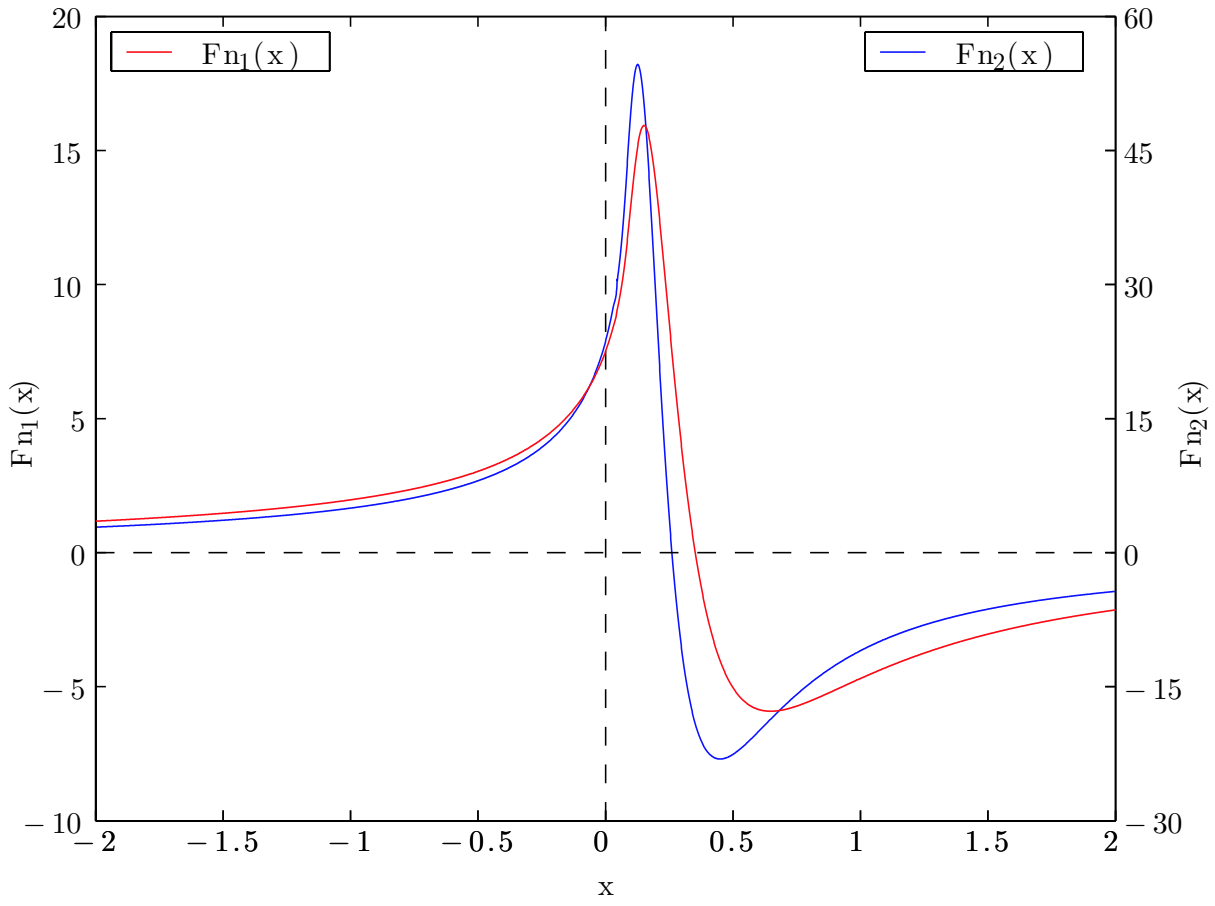

Figure B.1: $Fn_1(x)$ **and** $Fn_2(x)$ **around** $x = 0$**.**
The red curve (left axis) plots $\mathrm{Fn}_1(\mathrm{x})$, the blue (right axis) $\mathrm{Fn}_2(\mathrm{x})$.

```
k2spacing=1./numpitchanglepoints;

disp('initialisation of the grid')
r_base=(0.:rspacing:r_1);
k2_base=(0.:k2spacing:1.);
r=repmat(r_base,length(k2_base),1);
dr=rspacing.*ones(size(r));
R=R_0+r;

k2=repmat(k2_base',1,length(r_base));
dk2=k2spacing.*ones(size(k2));

q_0=0.7;
c=1.33; d=9.09; % the following should be modified
%q=q_0+(1-q_0).*r.^2;
q=q_0*(1+d*(r/a).^(2*c)).^(1/c);
%dq_dr=2*(1-q_0).*r;
dq_dr=(q_0/c).*(2*c*d*(r/a).^(2*c-1)).*(1+d*(r/a).^(2*c)).^((1/c)-1);
s=(r./q).*dq_dr;

%toroidal magnetic field profile B_phi(r)
```

```
B=B_0*(R_0./R);
dB_dr=-B_0*R_0*(R).^(-2);
dp_dr=-B.*dB_dr/mu_0;
%correction due to the shift of magnetic flux surfaces
eta=-2.*R.*mu_0.*dp_dr.*(q.^2)./(B.^2);

%plasma rotation
%Omega_0=28E3;
Omega_0=0;
Omega=Omega_0*(1-(2*r./a).^2);

%normalization
T_i0=2; %central ion temperature, keV
T_ia=0.050; %limiter temperature, keV
T_i=T_i0*(1-(r./a).^2) + T_ia; % keV
dT_idr=-2*T_i0.*r/a^2; % radial derivative of the ion temperature
n_i0=4; % central ion density in 1E-19 m^3
nu_n=6;
n_i=n_i0*((1-(r./a).^2)).^nu_n;
dn_idr=-6*n_i0.*r.^5/a^6; % radial derivative of the ion density

% code

disp('evaluating auxiliary functions')
disp('f_1(r) and f_2(r)')

%f_1(q), f_2(q)
f_1=(pi/2)*(1.0841-0.3193.*(1-q).^2-0.0683.*(1-q).^4);
f_2=5.1*(q-(1/2)).*((1-q).^2).*(1-0.034*(1-q));

disp('ellyptic integrals')
%k2 is k^2, colon vector with elements 0:1
[K,E] = ellipke(k2);

disp('F_1(k^2), F_2(k^2) and F_3(k^2)')
%F_1..F_3, dimension k^2
F_1=2.*(E./K) - 1;
F_2=2.*(E./K) + 2.*(k2 - 1);
F_3=(4./3).*( (2.*k2 - 1).*(E./K) + (1 - k2) );
plot(k2,F_1,k2,F_2,k2,F_3)
title('functions F_1, F_2 and F_3 defined by equation 6.23')
ylabel('F_j, j=1..3')
xlabel('k^2')

disp('F_q(r,k^2)')
%F_q: size (r x k^2)
F_q=2*E-K-(4*(1-q).*cos(pi*q)./(1-4*(1-q).^2)).*(E+(k2-1).*K) ...
    -(1+cos(pi*q)).*f_1.*(E+(k2-1).*K+2*E./pi - 1) ...
    -(1+cos(pi*q)).*(E-K) ...
```

```
    -f_2.*(1-k2).*(pi/2 - K);

%x(r,k^2)
%r-coordinates: q, Ti, s, eta, omegatot

% this is the iteration parameter
omega=10.^(-1:0.01:2.5);
omega=omega';
omega_0_tot=omega-Omega_0/1000;

figure(1)
set(0,'DefaulttextInterpreter','none')
subplot(8,2,1),plot(r(1,:),q(1,:)),xlabel('r [m]'),
ylabel('q(r)');title('safety factor q')
subplot(8,2,2),plot(r(1,:),dq_dr(1,:)),xlabel('r [m]'),
ylabel('dq/dr(r)');title('dq/dr')
subplot(8,2,3),plot(r(1,:),s(1,:)),xlabel('r [m]'),
ylabel('s(r)');title('plasma shear s(r)')
subplot(8,2,4),plot(r(1,:),B(1,:)),xlabel('r [m]'),
ylabel('B$_\phi$(r) [T]');title('toroidal magnetic field B$_\phi$(r)')
subplot(8,2,5),plot(r(1,:),dB_dr(1,:)),xlabel('r [m]'),
ylabel('dB/dr');title('dB/dr')
subplot(8,2,6),plot(r(1,:),dp_dr(1,:)),xlabel('r [m]'),
ylabel('dp/dr');title('derivative of plasma pressure')
subplot(8,2,7),plot(r(1,:),eta(1,:)),xlabel('r [m]'),
ylabel('$\zeta$');title('$\zeta$')
subplot(8,2,8),plot(r(1,:),Omega(1,:)),xlabel('r [m]'),
ylabel('$\Omega$(r)');title('plasma rotation')
subplot(8,2,9),plot(r(1,:),T_i(1,:)),xlabel('r [m]'),
ylabel('T$_i$(r) [keV]');title('T$_i$')
subplot(8,2,10),plot(r(1,:),dT_idr(1,:)),xlabel('r [m]'),
ylabel('dT$_i$/dr(r)');title('dT$_i$/dr')
subplot(8,2,11),plot(r(1,:),n_i(1,:)),xlabel('r [m]'),
ylabel('n$_i$(r) [10$^{-19}$ m$^{-3}$]');title('n$_i$')
subplot(8,2,12),plot(r(1,:),dn_idr(1,:)),xlabel('r [m]'),
ylabel('n$_i$(r)/dr');title('dn$_i$/dr')
drawnow
mattola('input',6,-1,-1,1,1)

disp('interpolation of resonant parameter domain')

return

for ff=1:length(omega) % normalzed to 1E3 r*s-1

omega_tot=omega(ff)-Omega/1000;

xmatrix=q.*T_i.*(F_1 + 2.*s.*F_2 - eta.*(1./(4.*q.*q) + F_3))...
    ./(B_0*R_0*Z_eff.*r.*omega_tot);
```

```
Fn_1=NaN*ones(size(xmatrix));
Fn_2=NaN*ones(size(xmatrix));
Fn_3=zeros(size(xmatrix));
Fn_4=zeros(size(xmatrix));

Fn_3(find(xmatrix>0))=(1./(xmatrix(find(xmatrix>0)).^(7/2)))...
    .*exp(-1./xmatrix(find(xmatrix>0)));
Fn_4(find(xmatrix>0))=(1./(xmatrix(find(xmatrix>0)).^(9/2)))...
    .*exp(-1./xmatrix(find(xmatrix>0)));

for line=1:size(xmatrix,1) % iteration in k^2

fullx=xmatrix(line,:);

chooser=setdiff(find(fullx>0.0015),find(fullx>0.029 & fullx<0.046));
if ~isempty(chooser)
  x=fullx(chooser);
  Fn_1(line,chooser)=4*sqrt(pi)*(1./x.^(7/2)).*(erfi(1./sqrt(x)))...
      .*exp(-1./x)-(3./x)-(2./x.^2)-(4./x.^3);
  Fn_2(line,chooser)=4*sqrt(pi)*(1./x.^(9/2)).*(erfi(1./sqrt(x)))...
      .*exp(-1./x)-(15./(2*x))-(3./x.^2)-(2./x.^3)-(4./x.^4);
end

chooser=find(fullx>0.029 & fullx<0.046);
if ~isempty(chooser)
  x=fullx(chooser);
  xbase=[0.02:0.001:0.029  0.046:0.001:0.055];
  Fn_1base=4*sqrt(pi)*(1./xbase.^(7/2))...
      .*(erfi(1./sqrt(xbase)))...
      .*exp(-1./xbase)-(3./xbase)-(2./xbase.^2)-(4./xbase.^3);
  Fn_2base=4*sqrt(pi)*(1./xbase.^(9/2))...
      .*(erfi(1./sqrt(xbase)))...
      .*exp(-1./xbase)-(15./(2*xbase))-...
      (3./xbase.^2)-(2./xbase.^3)...
      -(4./xbase.^4);
  Fn_1(line,chooser)=interp1(xbase,Fn_1base,x,'cubic');
  Fn_2(line,chooser)=interp1(xbase,Fn_2base,x,'cubic');

end

chooser=find(fullx<-0.0015);
if ~isempty(chooser)
  x=fullx(chooser);
  Fn_1(line,chooser)=-4*sqrt(pi)*(1./(-x).^(7/2)).*(erfc(1./sqrt(-x)))...
      .*exp(-1./x)-(3./x)-(2./x.^2)-(4./x.^3);
  Fn_2(line,chooser)=4*sqrt(pi)*(1./((-x).^(9/2))).*(erfc(1./sqrt(-x)))...
      .*exp(-1./x)-(15./(2.*x))-(3./(x.^2))-(2./(x.^3))-(4./(x.^4));
end
```

```
chooser=find(fullx>=-0.0015 & fullx<=0.0015);
%chooser=find(xmatrix==0);
if ~isempty(chooser)
  x=fullx(chooser);
  xbaseleft=[-0.02:0.001:-0.002];
  xbaseright=[0.002:0.001:0.02];
  Fn_1baseleft=-4*sqrt(pi)*(1./(-xbaseleft).^(7/2))...
      .*(erfc(1./sqrt(-xbaseleft)))...
      .*exp(-1./xbaseleft)-(3./xbaseleft)-(2./xbaseleft.^2)...
      -(4./xbaseleft.^3);
  Fn_2baseleft=4*sqrt(pi)*(1./((-xbaseleft).^(9/2)))...
      .*(erfc(1./sqrt(-xbaseleft)))...
      .*exp(-1./xbaseleft)-(15./(2.*xbaseleft))-...
      (3./(xbaseleft.^2))-(2./(xbaseleft.^3))-(4./(xbaseleft.^4));
  Fn_1baseright=4*sqrt(pi)*(1./xbaseright.^(7/2))...
      .*(erfi(1./sqrt(xbaseright)))...
      .*exp(-1./xbaseright)-(3./xbaseright)-...
      (2./xbaseright.^2)-(4./xbaseright.^3);
  Fn_2baseright=4*sqrt(pi)*(1./xbaseright.^(9/2))...
      .*(erfi(1./sqrt(xbaseright)))...
      .*exp(-1./xbaseright)-(15./(2*xbaseright))-...
      (3./xbaseright.^2)-(2./xbaseright.^3)-(4./xbaseright.^4);
  xbase=[xbaseleft 0 xbaseright];
  Fn_1base=[Fn_1baseleft 15/2 Fn_1baseright];
  Fn_2base=[Fn_2baseleft 105/4 Fn_2baseright];
  Fn_1(line,chooser)=interp1(xbase,Fn_1base,x,'cubic');
  Fn_2(line,chooser)=interp1(xbase,Fn_2base,x,'cubic');
end

end

Fn_1=real(Fn_1);
Fn_2=real(Fn_2);

disp(sprintf('integration for data point %i/%i',ff,length(omega)))
integrand1=(F_q.*F_q.*Fn_1.*dk2)./K;
integrand1(find(isnan(integrand1)))=0;
G_1=sum(integrand1);
integrand2=(F_q.*F_q.*Fn_2.*dk2)./K;
integrand2(find(isnan(integrand2)))=0;
G_2=sum(integrand2);
integrand3=(F_q.*F_q.*Fn_3.*dk2)./K;
integrand3(find(isnan(integrand3)))=0;
G_3=sum(integrand3);
integrand4=(F_q.*F_q.*Fn_4.*dk2)./K;
integrand4(find(isnan(integrand4)))=0;
G_4=sum(integrand4);
```

```
G_1=repmat(G_1,length(k2_base),1);
G_2=repmat(G_2,length(k2_base),1);
G_3=repmat(G_3,length(k2_base),1);
G_4=repmat(G_4,length(k2_base),1);

realdeltaWki=(e*mu_0*1E22/(3*sqrt(2)*pi))/(B_0*B_0*(epsilon_1^(3/2))*...
    (r_1^(5/2))).*  ...
    sum(dr.*sqrt(r).*(...
        ((q.*T_i./(B_0*Z_eff*omega_tot))...
    .*(T_i.*dn_idr-(3./2).*n_i.*dT_idr)  ...
    + n_i.*T_i.*r ).*G_1 + ...
        (q.*n_i.*T_i./(B_0*Z_eff*omega_tot))...
    .*dT_idr.*G_2 )  ,2);

imagdeltaWki=-(2*sqrt(2)*e*mu_0*1E22/(3*sqrt(pi)))/...
    (B_0*B_0*(epsilon_1^(3/2))*(r_1^(5/2))).*  ...
    sum(dr.*sqrt(r).*(...
        ((q.*T_i./(B_0*Z_eff*omega_tot))...
    .*(T_i.*dn_idr-(3./2).*n_i.*dT_idr) + n_i.*T_i.*r ).*G_3 + ...
        (q.*n_i.*T_i./(B_0*Z_eff*omega_tot)).*dT_idr.*G_4 )  ,2);

% plotting
finalrealdeltaWki(ff)=realdeltaWki(1);
finalimagdeltaWki(ff)=imagdeltaWki(1);
end

figure(2)
plot(log(omega),finalrealdeltaWki,log(omega),-finalimagdeltaWki)
set(0,'DefaultTextInterpreter','none')
plot(log(omega),finalrealdeltaWki,'g')
hold on
plot(log(omega),-finalimagdeltaWki,'b')
plot(log(omega),0,'k')
ax=axis;
ax(1)=min(log(omega));
ax(2)=max(log(omega));
axis(ax);
xlabel('log$_{10}$($\omega$)')
ylabel('$\delta$W$_k$')
legend('$\Re$($\delta$W$_k$)','-$\Im$($\delta$W$_k$)',2)
save results omega finalrealdeltaWki finalimagdeltaWki
disp('finished')

return
set(0,'DefaulttextInterpreter','none')
mattola('deltawk',6,-1,-1,1,1)

md=2.0147*1.660539E-27; %kg
ne_mean=2E19;
```

```
rho=ne_mean*md;
vA=B_0/sqrt(rho*mu_0)
omegaA=vA/R_0
sigma=(1/(r_1)^4)*sum( (r(1,:)).^3 .*( (1./q(1,:).^2) - 1 ) ...
    .* dr(1,:),2 );
betap=-2*mu_0/(B_0*B_0*epsilon_1*epsilon_1*r_1*r_1)...
    *sum(r(1,:).^2 .*10.*dp_dr(1,:) .* dr(1,:),2);
DELTA=epsilon_1*(betap+sigma+1/4);
DELTA=0.5 + 1.6/sqrt(epsilon_1)
omegastarpi=0.1*dp_dr(1,length(r))/(e*Z_eff*1E19*...
    n_i(1,length(r))*B_0*r(1,length(r)));
qq=s(1,length(r))*sqrt(1+DELTA)*sqrt(omega.*1000...
.*(omega.*1000-omegastarpi))/(3*pi*omegaA*(r(1,1001)/R_0)^2);
figure(3)
plot(log(omega),qq,'k')
```

Appendix C

Matlab error function for complex arguments

Matlab does not include the complex error function $erfi(x)$. The code makes use of the identity $erfi(x) = -ierf(ix)$, but unfortunately the Matlab error function does not permit the calculation with complex arguments.

The following algorithm was therefore used to calculate $erf(z)$ for $z \in \mathbb{C}$. This is essentially a Matlab implementation of the Fortran algorithm listed in [8]

C.1 Imaginary error function erfi(x)

Listing C.1: Imaginary error function $erfi(x)$

```
function [cer]=erfi(z);
% Calculation of the imaginary error function
% of complex arguments erfi(z).
% property: erfi(z) = -i*erf(iz)
%
% Input : z   --- Complex argument
% Output: CER --- erfi(z)
%
% This algorithm is a Matlab implementation of the code
% given in Shan jie Zhang and Jianming Jin, Computation
% of special functions, John Wiley, New York, 1996.
%
% Centre de Recherches en Physique des Plasmas (CRPP)
% Ecole polytechnique federale de Lausanne, Switzerland
%
% Christian SCHLATTER, 27 of sepetember, 2004
% Revision 1.0

z=i.*z;
a0=0;pi=0;

a0=abs(z);
c0=exp(-z.*z);
```

```
pi=3.1415926535897793d0;
z1=z;
z1(find(real(z) < 0.0))=-z(find(real(z) < 0.0));
index1=find(a0 <= 5.8);
%save temp index1
cs(index1)=z1(index1);
cr(index1)=z1(index1);
for   k=1:120;
cr(index1)=cr(index1).*z1(index1).*z1(index1)./(k+0.5d0);
cs(index1)=cs(index1)+cr(index1);
if (max(abs(cr(index1)./cs(index1))) < 1.0d-15) break; end;
end;
cer(index1)=2.0d0.*c0(index1).*cs(index1)./sqrt(pi);

index2=setdiff(1:length(z),index1);
cl(index2)=1.0d0./z1(index2);
cr(index2)=cl(index2);
for   k=1:13;
cr(index2)=-cr(index2).*(k-0.5d0)./(z1(index2).*z1(index2));
cl(index2)=cl(index2)+cr(index2);
if (max(abs(cr(index2)./cl(index2))) < 1.0d-15) break; end;
end;
cer(index2)=1.0d0-c0(index2).*cl(index2)./sqrt(pi);
cer(find(real(z) < 0.0))=-cer(find(real(z) < 0.0));
cer=-i.*cer;
return;
```

Bibliography

[1] Milton Abramowitz, *Handbook of mathematical functions*, Dover Publications, New York, 1972.

[2] I. B. Bernstein, E. A. Frieman, M. D. Kruskal, and R. M. Kulsrud, *An energy principle for hydromagnetic stability problems*, Proceedings of the Royal Society of London. Series A, Mathematical and Physical Sciences **244** (1958), no. 1236, 17–40.

[3] A. Bondeson and M. N. Bussac, *Stability of the n=1 ideal internal kink for large aspect ratio shafranov equilibria*, Nucl. Fus. **32** (1992), no. 3, 513.

[4] M. N. Bussac, R. Pellat, D. Edery, and J. L. Soulé, *Internal kink modes in toroidal plasmas with circular cross sections*, Phys. Rev. Lett. **35** (1975), no. 24, 1638–1641.

[5] D. J. Campbell, J. G. Cordey, A. W. Edwards, R. D. Gill, E. Lazzaro, G. Magyar, A. L. McCarthy, J. O'Rourke, F. Pegoraro, F. Porcelli, P. Smeulders, D. F. H. Start, P. Stubberfield, J. A. Wesson, E. Westerhof, and D. Zasche, *Sawtooth activity and current density profiles in jet*, Plasma physics and controlled nuclear fusion research 1988 (Nice, France), International Atomic Energy Agency, International Atomic Energy Agency, Vienna, 1988, pp. 377–385.

[6] D. J. Campbell, D. F. H. Start, J. A. Wesson, D. V. Bartlett, V. P. Bhatnagar, M. Bures, J. G. Cordey, G. A. Cottrell, P. A. Dupperex, A. W. Edwards, C. D. Challis, C. Gormezano, C. W. Gowers, R. S. Granetz, J. H. Hammen, T. Hellsten, J. Jacquinot, E. Lazzaro, P. J. Lomas, N. Lopes Cardozo, P. Mantica, J. A. Snipes, D. Stork, P. E. Stott, P. R. Thomas, E. Thompson, K. Thomsen, , and G. Tonetti, *Stabilization of sawteeth with additional heating in the jet tokamak*, Physical Review Letters **60** (1988), no. 21, 2148–2151.

[7] Jonathan Peter Graves, *Kinetic stabilisation of the internal kink mode for fusion plasmas*, Ph.D. thesis, School of Mathematical Sciences, Division of Theoretical Mechanics, University of Nottingham, December 1999.

[8] Shan jie Zhang and Jianming Jin, *Computation of special functions*, John Wiley, New York, 1996.

[9] K. G. McClements, R. O. Dendy, C. G. Gimblett, R. J. Hastie, and T. J. Martin, *Stabilization of the ideal m=1 internal kink by alpha particles and icrf heated ions*, Nucl. Fus. **35** (1995), no. 12, 1761–1768.

[10] M. N. Rosenbluth, P. Y. Dagazian, and P. H. Rutherford, *Nonlinear properties of the internal m = 1 kink instability in the cylindrical tokamak*, Physics of fluids **16** (1973), no. 11, 1894–1902.

[11] John Wesson, *Tokamaks*, Clarendon Press, Oxford, 2004.

[12] R. B. White, P. H. Rutherford, P. Colestock, and M. N. Bussac, *Sawtooth stabilization by energetic trapped particles*, Physical Review Letters **60** (1988), no. 20, 2038–2041.